J Mater Sci: Mater Electron (2021) 32:8648–8656

Enhanced red photoluminescence in chain-like $SrAl_2O_4:Eu^{3+}$ nanophosphors: utilizing charge compensation by modulating Na^+ co-doping concentration

Arnab De[1], Arnab Kumar Dey[1,2], Bibek Samanta[1,3], and Uttam Kumar Ghorai[1,*]

[1] *Department of Industrial & Applied Chemistry, Swami Vivekananda Research Centre, Ramakrishna Mission Vidyamandira, Belur Math, Howrah 711202, India*

[2] *Present address: Department of Materials Science and Engineering, IIT Delhi, Delhi 110016, India*

[3] *Present address: Department of Metallurgical Engineering & Materials Science, IIT Bombay, Mumbai 400076, India*

Received: 10 May 2020
Accepted: 4 October 2020
Published online: 18 March 2021

ABSTRACT

In the recent days, rare-earth doped phosphors have attracted an immense attraction in luminescence field for various solid-state lighting and electronic display device applications. However, need of efficient red phosphor is a prevalent challenge in this field. Herein, we report a bright red light emitting Na^+ co-doped $SrAl_2O_4:Eu^{3+}$ phosphor which is synthesized by modified sol–gel technique. These nanophosphors show excellent red emission due to characteristic $^5D_0 \rightarrow {}^7F_j$ (j = 1, 2, 3, 4) transitions of the doped Eu^{3+} ions excited by 394 nm. Photoluminescence studies of both Eu^{3+} doped $SrAl_2O_4$ and Na^+ co-doped $SrAl_2O_4:Eu^{3+}$ has shown more than fourfold increase in the intensity for optimum Na^+ addition. The improved decay time obtained from decay measurement has revealed that the co-doped Na^+ has successfully reduced the nonradiative transitions. Thus, addition of monovalent Na^+ to Eu^{3+} doped $SrAl_2O_4$ was found to be effective to address the charge imbalance problem along with significant enhancement in luminescence intensity and decay time. The results suggest that this nanophosphor could be a major candidate in the rapidly increasing field of solid-state lighting applications.

Address correspondence to E-mail: uttamindchem00@gmail.com

https://doi.org/10.1007/s10854-021-05524-2

1 Introduction

The ever-increasing demand of energy-efficient solid-state lighting, especially in high quality displays and household lights have propelled the scientific society towards developing high quality phosphors. These phosphors are widely used in various fields like white light emitting diodes (WLEDs), plasma display panels (PDPs), and field emission displays (FEDs) [1–3]. Among these, white LEDs have gathered considerable attraction as fourth-generation lighting source due to its superiority over present incandescent and fluorescent lamps [4–6]. An emerging route of preparing WLEDs consists of utilizing ultraviolet (UV) emission of InGaN chips to excite different phosphors. A suitable mixing of three elementary colors, i.e. red, green, and blue from proper UV-excited phosphors can generate the required white color [7–10]. However, the poor efficiency of the red part with respect to the blue and green counterpart is a major disadvantage of this method. Thus, the preparation of a suitable and efficient red phosphor excited by UV light is still a major challenge in this field.

Rare-earth (RE) ions doping as luminescent centers in proper host material has always been the most practiced way to obtain outstanding phosphor materials [11–14]. Among various RE ions present, trivalent europium (Eu^{3+}) ion is the most utilized one regarding its characteristic red emission ($^5D_0 \rightarrow {}^7F_2$) under UV excitation [15–18]. As the transfer of absorbed energy from the host material to RE ions is essential for realizing bright luminescence, wide band gap, and low phonon losses from the host are essential for excellent luminescence properties of the phosphor [19, 20]. In this regard, alkaline earth aluminate materials have gathered significant attention in the recent days [21–24]. Among them, $SrAl_2O_4$ is a widely studied material due to its stable structure, chemical resistance, low toxicity, and excellent optical properties [25–29]. Owing to wide band gap ($\sim$ 6.6 eV) [30, 31], $SrAl_2O_4$ does not absorb in the entire visible spectra, which theoretically eliminates the probability of re-absorption of the emitted lights from the RE ions. The low phonon energy ($\sim$ 470–480 cm^{-1}) [32] of the host also reduces the chances of non-radiative losses.

From application point of view, the nanophosphors can be coated on a substrate with considerably greater homogeneity and controlled thickness than the bulk phosphor. Another well-recognized phenomenon is that the photoluminescence (PL) intensity of RE doped phosphors increases with increasing dopant concentration up to a certain concentration only [7]. Beyond this optimum concentration, some impurity phases are created or concentration quenching occurs. Thus, designing an efficient phosphor with enhanced PL intensity within the critical concentration is a difficult problem to solve.

In order to address the aforementioned demands, co-doping monovalent alkali metal ions (Li^+, Na^+, K^+) with the RE doped phosphors has been studied rigorously in recent years [33–35]. Although Eu^{3+} doped $SrAl_2O_4$ has been studied thoroughly, to the author's best knowledge, there is no report on Na^+ co-doped $SrAl_2O_4$:Eu^{3+} nanophosphors synthesized by sol–gel route. Herein, we have reported Na^+ co-doped $SrAl_2O_4$:Eu^{3+} nanophosphors synthesized via modified citrate–nitrate type sol–gel method. Extensive study of the PL property of both $SrAl_2O_4$:Eu^{3+} and Na^+ co-doped $SrAl_2O_4$:Eu^{3+} nanophosphors over a range of Na^+ concentration has shown more than four times enhancement in PL intensity with optimum Na^+ co-doping. Thus, these results may offer an attractive alternate for addressing the challenges regarding red LEDs in day-to-day solid-state lighting applications.

2 Experimental sections

2.1 Synthesis of $SrAl_2O_4$:Eu^{3+} and Na^+ doped $SrAl_2O_4$:Eu^{3+} nanophosphors

The targeted $SrAl_2O_4$: x% Eu^{3+} (x = 0, 1, 2, 3, 4) and $SrAl_2O_4$: 3% Eu^{3+}, y% Na^+ (y = 1, 2, 3) nanophosphors were prepared using a modified sol–gel method [35]. The chemicals used were $Sr(NO_3)_2$ (Merck 99.9%), $Al(NO_3)_3 \cdot 9H_2O$ (Merck, 99.9%), Eu_2O_3 (Sigma-Aldrich 99.99%), HNO_3, $NaNO_3$ (Merck 99.9%), citric acid (Merck 99.9%), and ethylenediamine (Merck 99.9%). $Eu(NO_3)_3$ was prepared by dissolving Eu_2O_3 in HNO_3 in proper stoichiometry. All chemicals were analytical grade and used without further purification. For synthesis, stoichiometric amount of $Sr(NO_3)_2$, $Al(NO_3)_3 \cdot 9H_2O$, $Eu(NO_3)_3$ and $NaNO_3$ were taken in 35 mL DI water and the solution was magnetically stirred for 1 h. Then, the aqueous citric acid solution was added drop by drop to the above metal nitrate solution in

molar ratio of $Cit^{3-}/(Sr^{2+} + Al^{3+}) = 1$. This solution was magnetically stirred for 30 min to get a homogeneous and transparent solution. pH of this solution was adjusted to 8 by ethylenediamine. The solution was slowly evaporated using a hot water bath, which converted the solution to a highly viscous colloidal gel. In subsequent steps, the gel was dried in oven at 120 °C for overnight and then it was calcined at 500 °C for 4 h to get rid of the organics. Finally, the obtained porous material was finely ground using mortar pestle and the powder was annealed at 1000 °C for 3 h in a muffle furnace to get the ultrafine Eu^{3+} doped and Na^+ co-doped $SrAl_2O_4$ powders. The Eu^{3+} doped $SrAl_2O_4$ nanophosphors were synthesized following the same procedure, but $NaNO_3$ was not added this time.

2.2 Characterization

For crystal structure and phase detection, the synthesized nanophosphors were analyzed using Bruker D8 ADVANCED ECO diffractometer with monochromatic Cu K_α radiation (λ = 1.5406 Å). The generator power was 40 kV and current was 25 mA for the experiment. The FTIR studies were performed using a Shimadzu IRAffinity-1S FTIR spectrophotometer. The microstructural analysis was done by HRTEM (FEG-TEM, JEOL-JEM 2100F). The photoluminescence properties were studied by Edinburgh FLS 980 Spectrofluorometer with Xenon lamp as the excitation source. CIE chromaticity coordinates of the nanophosphors were determined using 1931 CIE chromaticity theory.

3 Results and discussion

3.1 Structural, microstructural, and compositional analysis

3.1.1 XRD analysis

The X-ray diffractogram of $SrAl_2O_4:Eu^{3+}$ and Na^+ co-doped $SrAl_2O_4:Eu^{3+}$ nanophosphors are represented in Fig. 1a and c, respectively. The diffraction patterns reveal that all the obtained nanophosphors were monoclinic with $P2_1$ space group (JCPDS card number 34–0379). Six major peaks of $SrAl_2O_4$ were found at 2θ positions 20.06°, 22.81°, 28.56°, 29.32°, 29.73° and 35.09° corresponding (011), (120), ($\bar{2}$11), (220), (211) and (031), respectively. Doped Eu^{3+} occupies the Sr^{2+} sites in $SrAl_2O_4$ structure. Substitution of smaller of Eu^{3+} (0.95 Å) ion in Sr^{2+} (1.18 Å) leads to the shrinkage of the unit cell which is in accordance with the observed higher angle shifting of the characteristic peak near 2θ = 20.06° as shown in Fig. 1b. There was no trace of excess Eu^{3+} in $SrAl_2O_4:Eu^{3+}$ up to 4% Eu^{3+} which indicates proper incorporation of Eu^{3+} in the host. Due to comparable sizes of Sr^{2+} and Na^+ (1.18 and 1.02 Å, respectively), Na^+ also goes to Sr^{2+} sites in the $SrAl_2O_4$ lattice.

As presented in Fig. 1c, XRD patterns of Na^+ co-doped $SrAl_2O_4:Eu^{3+}$ shows that there was no trace of excess Na^+ up to 3% Na^+ addition. This co-doped Na^+ occupies the vacant Sr^{2+} sites, which solves the charge imbalance problem created by doping of Eu^{3+} in Sr^{2+} sites. Initially, the co-doping of Na^+ leads to increased crystallinity of the nanophosphor. But this enhancement is only up to a certain Na^+ concentration. Above this concentration, decrease in crystallinity with increasing Na^+ is observed due to defects introduced by excess Na^+ ions incorporated.

3.1.2 Microstructural Study

Figure 2 represents the TEM micrograph of the synthesized Na^+ co-doped $SrAl_2O_4:Eu^{3+}$ nanophosphor. As presented in Fig. 2a–b, an interconnected chain-like morphology is observed for the synthesized phosphors. Figure 2c shows that the average chain diameter was found to be in the range of 100–150 nm. Figure 2d clearly shows the array of atoms present in the phosphor. A portion of the atoms belong to the (011) plane with an interplanar spacing of 0.44 nm as indicated in Fig. 2d.

3.1.3 FTIR study

As shown in Fig. 3, vibration stretching frequencies between 700 and 1000 cm^{-1} are related to Sr–O–Al and Al–O bond vibrations. Sr–O anti-symmetric stretching vibrations are present in frequencies between 500 and 650 cm^{-1}. Thus, the formation of the polyhedrons confirmed by the metal-oxide stretching frequencies indicates the formation of $SrAl_2O_4$ [27].

3.2 Spectroscopic analysis

The PL excitation and emission spectra of both $SrAl_2O_4$: Eu^{3+} and Na^+ co-doped $SrAl_2O_4$: Eu^{3+}

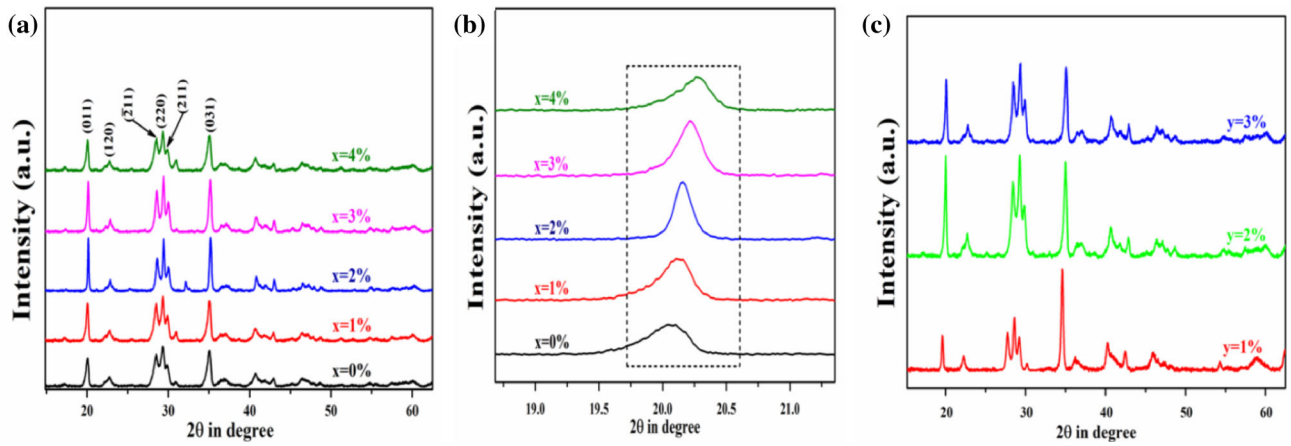

Fig. 1 **a** XRD patterns of synthesized $SrAl_2O_4$: xEu^{3+} (x = 0%, 1%, 2%, 3%, 4%) nanophosphors. **b** Higher angle peak shifting in $SrAl_2O_4$:Eu^{3+} nanophosphors with increasing Eu^{3+}concentration. **c** XRD patterns of synthesized $SrAl_2O_4$: 3%Eu^{3+}, yNa^{+} (y = 1%, 2%, 3%) nanophosphors

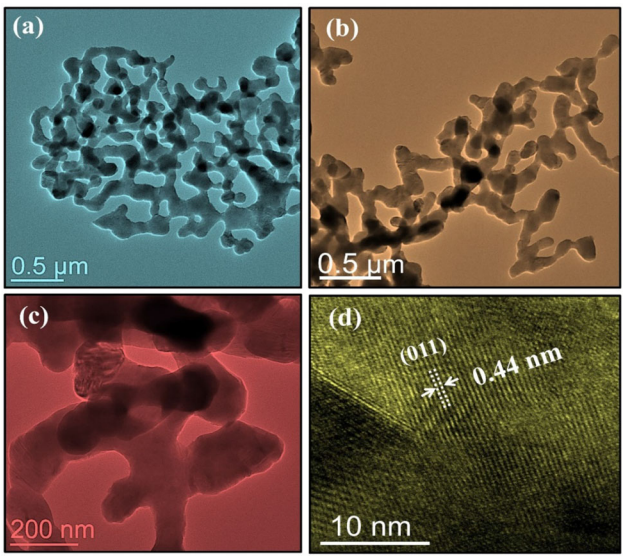

Fig. 2 **a**–**c** TEM micrographs of $SrAl_2O_4$: 3%Eu^{3+}, 2%Na^{+}. **d** HRTEM micrograph showing lattice fringes with interplanar spacing

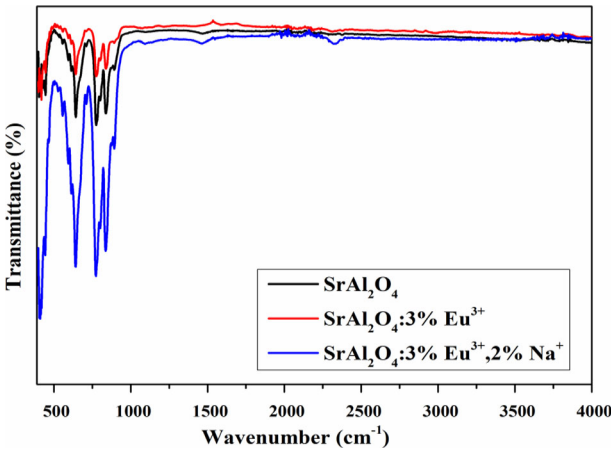

Fig. 3 FTIR spectra of $SrAl_2O_4$, $SrAl_2O_4$: 3%Eu^{3+} and $SrAl_2O_4$: 3%Eu^{3+}, 2%Na^{+}

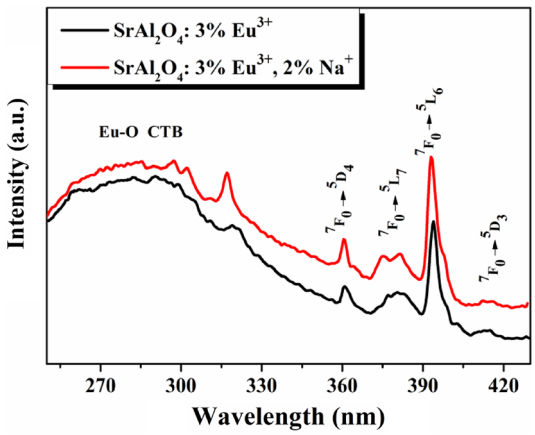

Fig. 4 PL excitation spectra of the $SrAl_2O_4$: 3% Eu^{3+} and $SrAl_2O_4$: 3% Eu^{3+}, 2% Na^{+} nanophosphors monitored at 616 nm emission

nanophosphors were studied. PL excitation spectra of the 3% Eu^{3+} doped $SrAl_2O_4$ and 3% Eu^{3+}, 2% Na^{+} doped $SrAl_2O_4$ nanophosphors are presented in Fig. 4, which were recorded by monitoring the emission of Eu^{3+} at 616 nm.

As shown in Fig. 4, the excitation spectra have a broad peak at 285 nm and other narrow peaks were observed between 300 and 420 nm. In $SrAl_2O_4$, the 2p orbitals of O^{2-} form the valence band and the conduction band is composed of 4d orbitals of Sr^{2+} [26, 30]. The broad peak at 285 nm corresponds to the charge transfer band (CTB) due to transfer of

electrons from O^{2-} (2p) orbital to the empty states of the $4f^6$ orbital of Eu^{3+} (Eu^{3+}—O^{2-}transition). The excitation spectra also contain some other transitions between 300 and 420 nm arising from f–f transitions of the Eu^{3+} ions in the host lattice. These peaks, resulting from the direct excitation of the Eu^{3+} ground state to the higher levels in the $4f^6$ configuration, can be assigned as $^7F_0 \rightarrow {}^5D_4$ (361 nm), $^7F_0 \rightarrow {}^5L_7$ (382 nm), $^7F_0 \rightarrow {}^5L_6$ (394 nm), and $^7F_0 \rightarrow {}^5D_3$ (413 nm) transitions. Among these sharp peaks, the 394 nm wavelength peak exhibits the highest peak intensity. From the excitation spectra, it is also prominent that due to Na^+ co-doping the intensity of the excitation spectra increases, which in turn enhances the intensity of PL emission. The strong excitation peak at 394 nm would enable this nanophosphor to be potentially used in UV-LEDs.

Room temperature PL emission spectra of $SrAl_2O_4$:Eu^{3+} and Na^+ co-doped $SrAl_2O_4$:Eu^{3+} nanophosphors, excited by 394 nm wavelength, are represented in Fig. 5a and b, respectively. In this configuration, the crystal field exerted by coordinating O^{2-} splits the energy levels of Eu^{3+}. This splitting leads to formation of sharp and intense emission lines between 580 and 710 nm for both Eu^{3+} doped and Eu^{3+} doped, Na^+ co-doped samples. Four sharp peaks present in the emission spectra at 587, 616, 649 and 701 nm occur due to the transitions $^5D_0 \rightarrow {}^7F_j$, j = 1,2,3,4 of the Eu^{3+} ions, respectively. The peak at 587 nm ($^5D_0 \rightarrow {}^7F_1$) is due to magnetic dipole transitions while the peak at 616 nm ($^5D_0 \rightarrow {}^7F_2$) is due to electric dipole transitions [34]. For Eu^{3+} doped samples, quenching of PL intensity was observed after 3% Eu^{3+} doping. This can be ascribed to concentration quenching by interaction of the Eu^{3+} ions with each other [34]. As shown in Fig. 5a and b, for the Eu^{3+} doped samples, the sample with the highest PL intensity is $SrAl_2O_4$:3%Eu^{3+} and for Na^+ co-doped $SrAl_2O_4$:Eu^{3+} phosphors, the sample with the highest PL intensity is $SrAl_2O_4$:3%Eu^{3+},2% Na^+. These two samples are referred to optimized samples.

3.2.1 *Photoluminescence mechanism*

Figure 6 is a schematic representation of the energy levels of Eu^{3+} and possible mechanism for photoluminescence in the synthesized phosphor. In $SrAl_2O_4$, O^{2-} ions form the valence band and Sr^{2+} ions form the conduction band [30]. A charge transfer band (CTB) is formed within the valence and conduction band due to electronic charge transfer from the 2p orbitals of O^{2-} ions to 4f orbitals of Eu^{3+} ions. The excitation process consists of two main pathways, one is the direct transfer of valence band electrons to the CTB and another is transferring the electrons to higher energy levels of Eu^{3+}. The first process takes place at 285 nm and the second one at 394 nm. In both processes, the excited electrons quickly jump to the lowest excited level ($^5D_0$) of Eu^{3+} via nonradiative transition, and then it makes 4 transitions to the lower energy levels. These four transitions give rise to four emission lines in the emission spectra at 587 nm, 616 nm, 649 nm, and 701 nm.

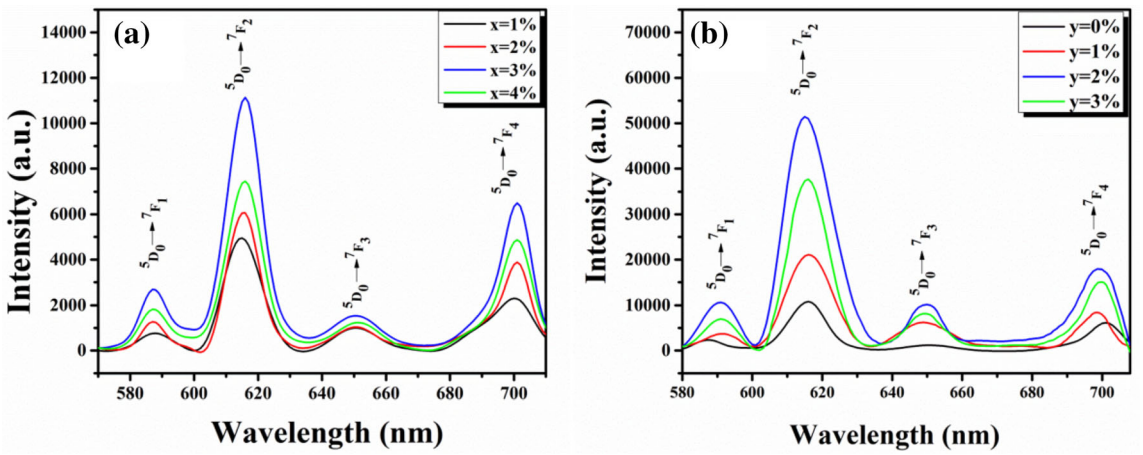

Fig. 5 Emission spectra of **a** $SrAl_2O_4$: xEu^{3+}. **b** $SrAl_2O_4$: 3%Eu^{3+}, yNa^+

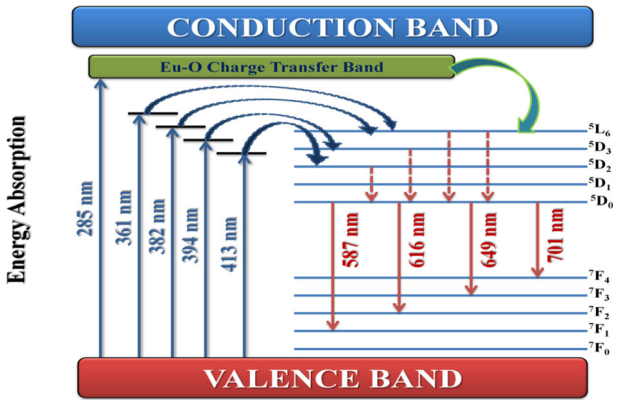

Fig. 6 Schematic representation of the energy levels showing possible luminescence mechanism in Eu^{3+} doped $SrAl_2O_4$ and Na^+co-doped $SrAl_2O_4$:Eu^{3+} nanophosphors

3.2.2 *Effect of Na^+ doping*

Emission spectra for different concentrations of co-doped Na^+ in $SrAl_2O_4$:3%Eu^{3+} is presented in Fig. 5b. There is no significant change in the position of the emission peak, but the emission intensity has increased significantly with increasing Na^+ concentration from 1 to 2% and the intensity is greatly enhanced than that of 3% Eu^{3+} doped $SrAl_2O_4$ nanophosphor. As shown in Fig. 5b, the luminescence intensity increased gradually with the increase in Na^+ concentration from 1 to 2% and then it decreased. From Fig. 5b, it can be seen that for optimum co-doped sample (2% Na^+) the emission intensity obtained was more than four times than the highest emission of optimum Eu^{3+} doped sample.

This can be ascribed to several reasons. Charge compensation is most important among them. When Eu^{3+} is doped in $SrAl_2O_4$ matrix, it substitutes the Sr^{2+} and this creates an extra positive charge for each substitution. To maintain the overall electroneutrality of the crystal, incorporation of two Eu^{3+} ions leads to elimination of three Sr^{2+} ions and formation of one Sr^{2+} vacancy as shown by Kröger–Vink notation:

$$3Sr_{Sr} \rightarrow 2Eu_{Sr}^{\cdot} + V_{Sr}'' \quad (1)$$

These cation vacancies reduce the luminescence intensity due to increase in non-radiative transition from Eu^{3+} luminescence centre to these Sr^{2+} vacancies. This problem can be effectively overcome by incorporating monovalent alkali metal ions by balancing the charge and number of sites simultaneously. Two Sr^{2+} sites are occupied by one Eu^{3+} and one Na^+. This can be represented by following notation:

$$Eu^{3+} + Na^+ \xrightarrow{2Sr_{Sr}} Eu_{Sr}^{\cdot} + Na_{Sr}' \quad (2)$$

But volume imbalance is created due to dissimilar ionic radii of host (Sr^{2+}) ion and Na^+ ion. Volume imbalance problem is not very significant up to a certain doping concentration of Na^+ ion. Beyond 2% Na^+ lattice distortion takes place and subsequently the luminescence intensity decreases due to decrease in crystallinity. Another important parameter that affects emission intensity $SrAl_2O_4$:Eu^{3+}, Na^+ nanophosphors is the formation of oxygen vacancies which are created by the replacement of Sr^{2+} by Na^+. Nature of the surrounding ions strongly regulate CT energy. As shown in the excitation spectra, broad band in the range of 250–310 nm has been observed due to the electron transfer from the filled 2p orbitals of the O^{2-} ions to the empty 4f shell of the Eu^{3+} ions (charge transfer transition). The created oxygen vacancies act as the sensitizer for the Eu^{3+} ions and cause a very efficient energy transfer to Eu^{3+} ions. As a result, emission intensity of Eu^{3+} gets enhanced due to effective energy transfer from host to activator. However, the amount of oxygen vacancies in the crystal becomes significant enough after 2% Na^+. As a result, the overall crystallinity decreases and the luminescence intensity decrease. The electric dipole transition at 616 nm maintains its dominance over 587 nm for both Eu^{3+} doped and Eu^{3+} doped Na^+ co-doped sample because Sr^{2+} is located at a low symmetry site.

Figure 7 indicates the CIE plot of both $SrAl_2O_4$: 3%Eu^{3+} and $SrAl_2O_4$: 3%Eu^{3+}, 2% Na^+ for comparison. The co-ordinates for both cases are shown in Table 1.

An increase in x coordinate with simultaneous decrease in y coordinate in the chromaticity diagram confirms the improved redness with addition of Na^+ ions. This improvement in redness makes it more suitable for its application in display and lighting purposes.

3.2.3 *Decay study*

The room temperature decay profile for the 616 nm emission of Eu^{3+} excited at 394 nm UV radiation was also studied as represented in Fig. 8.

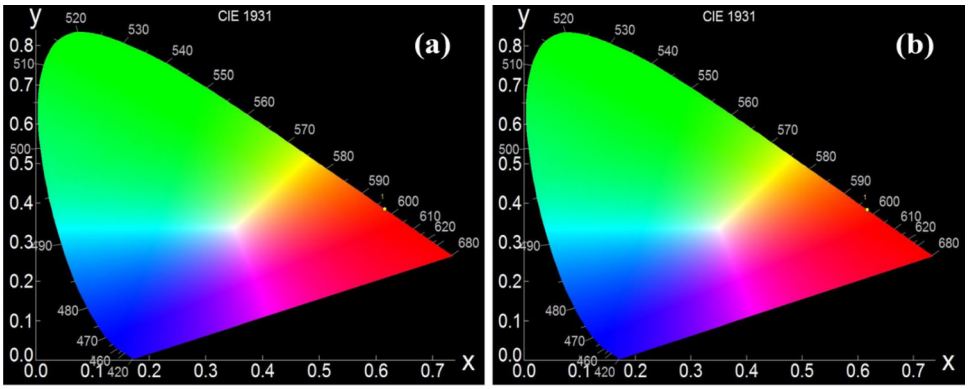

Fig. 7 CIE plot of **a** $SrAl_2O_4$: 3%Eu^{3+}. **b** $SrAl_2O_4$: 3%Eu^{3+}, 2% Na^+

Table 1 Color coordinates of the optimized samples

Sample	*x* Coordinate	*y* Coordinate
(1) $SrAl_2O_4$: 3%Eu^{3+}	0.61565	0.38388
(2) $SrAl_2O_4$: 3%Eu^{3+}, 2% Na^+	0.61697	0.38256

The decay curves of the $^5D_0 \rightarrow {}^7F_2$ transition for Eu^{3+} doped and Eu^{3+}, Na^+ co-doped nanophosphors were fitted into a bi-exponential and mono-exponential function, respectively. The bi-exponential decay equation (Eq. 3) and the monoexponential decay equation (Eq. 4) are given below

$$I(t) = A_1 e^{\left(-\frac{t}{\tau_1}\right)} + A_2 e^{\left(-\frac{t}{\tau_2}\right)}. \quad (3)$$

$$I(t) = I_0 e^{\left(-\frac{t}{\tau}\right)}. \quad (4)$$

where I_0 is the initial luminescence intensity, $I(t)$ is the luminescence intensity at time t, τ_1, and τ_2 represent components of luminescence decay time, A_1 and A_2 are the weighting parameters. For mono-exponential function, τ is the luminescence decay time. Eq. 5 was used to determine the average decay time of bi-exponential decay.

$$\tau_{avg} = \frac{A_1\tau_1^2 + A_2\tau_2^2}{A_1\tau_1 + A_2\tau_2}. \quad (5)$$

The average decay time for 616 nm from 3% Eu^{3+} doped nanophosphor is found to be 396 μs and the decay time for 3% Eu^{3+}, 2% Na^+ co-doped nanophosphor is found to be 559 μs. For the Eu^{3+} doped samples, the biexponential PL decay characteristics in our system may be arising due to non-uniform distribution of Eu^{3+} in the $SrAl_2O_4$ matrix [36]. For co-doped samples, the single exponential decay behaviour indicates that the coordination environment of the Eu^{3+} ion in $SrAl_2O_4$ matrix is homogeneous [37]. Enhancement in decay time after Na^+ codoping is an indication of reduction in the surface defects and nonradiative centers in the phosphor system [34]. A microsecond order decay time for all the samples confirms the suitability of the materials for utilizing in lighting applications.

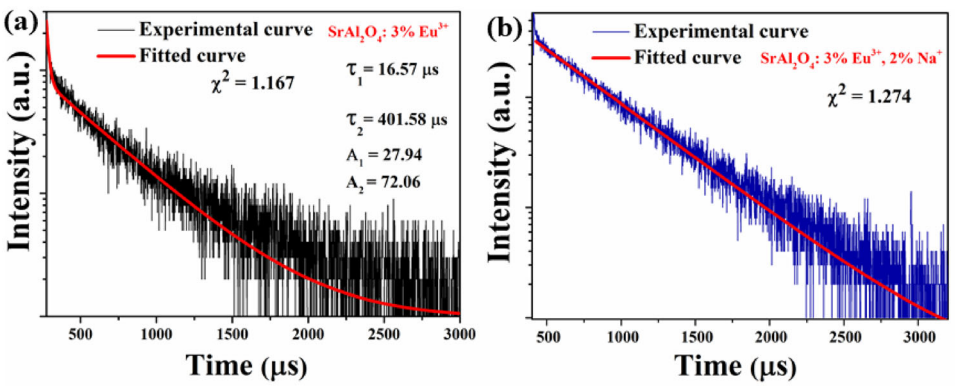

Fig. 8 Photoluminescence decay profile of **a** $SrAl_2O_4$:3%Eu^{3+}. **b** $SrAl_2O_4$:3%Eu^{3+},2% Na^+

4 Conclusions

In summary, a range of Eu^{3+} doped $SrAl_2O_4$ and Eu^{3+} doped, Na^+ co-doped $SrAl_2O_4$ was successfully synthesized via facile sol–gel method. These nanophosphors have shown bright red emission under 394 nm excitation due to $^5D_0 \rightarrow {}^7F_j$ (j = 1, 2, 3, 4) of Eu^{3+} substituted in the $SrAl_2O_4$ matrix. The intensity of red emission from Eu^{3+} doped $SrAl_2O_4$ was enhanced successfully via incorporation of Na^+ ions as evident in the corresponding photoluminescence emission spectra. This enhancement is attributed to the charge compensation and increase in crystallinity through addition Na^+ which subsequently reduces the amount of non-radiative centers in $SrAl_2O_4$ matrix. Photoluminescence decay study showed that the Na^+ co-doped sample has higher decay time which also supports the reduction of nonradiative centers in these phosphors. The amount of Eu^{3+} and Na^+ was optimized to be 3% and 2%, respectively (i.e. $SrAl_2O_4$:3%Eu^{3+} and $SrAl_2O_4$:3%-Eu^{3+}, 2%Na^+). Finally, the addition of Na^+ was found to be a successful method of improving the red emission of Eu^{3+} doped $SrAl_2O_4$ which can be possibly utilized in solid-state lighting applications.

Acknowledgements

UKG acknowledges the Teachers Associateship for Research Excellence (TARE) fellowship and research grant (TAR/2018/000763) of SERB, Govt. of India. UKG also acknowledges Science and Technology and Biotechnology Department, Govt. of West Bengal for proving the financial support [199 (Sanc.)/ST/P/S&T/6G-12/2018]. UKG also acknowledges the central DST-FIST programme (SR/FST/College-287/2015) and DBT star college scheme (BT/HRD/11/036/2019) for funding.

References

1. M. Shang, C. Li, J. Lin, How to produce white light in a single-phase host? Chem. Soc. Rev. **43**, 1372–1386 (2014)
2. Y. Zhang, Z. Wu, D. Geng et al., Full color emission in $ZnGa_2O_4$: simultaneous control of the spherical morphology, luminescent, and electric properties via hydrothermal approach. Adv. Funct. Mater. **24**, 6581–6593 (2014)
3. X. Li, Y. Zhang, D. Geng, $CaGdAlO_4$:Tb^{3+}/Eu^{3+}as promising phosphors for full-color field emission displays. J. Mater. Chem. C **2**, 9924–9933 (2014)
4. K. Li, S. Liang, M. Shang et al., Photoluminescence and energy transfer properties with Y+SiO_4 substituting Ba+PO_4 in $Ba_3Y(PO_4)_3$: Ce^{3+}/Tb^{3+}, Tb^{3+}/Eu^{3+} phosphors for w-LEDs. Inorg. Chem. **55**, 7593–7604 (2016)
5. K. Li, M. Shang, H. Lian et al., Recent development in phosphors with different emitting colors via energy transfer for FEDs and UV/n-UV w-LEDs. J. Mater. Chem. C **4**, 5507–5530 (2016)
6. S. Liang, M. Shang, H. Lian et al., Deep red MGe_4O_9:-Mn^{4+}(M = Sr, Ba) phosphors: structure, luminescence properties and application in warm white light emitting diodes. J. Mater. Chem. C **4**, 6409–6416 (2016)
7. B. Samanta, A.K. Dey, P. Bhaumik et al., Controllable white light generation from novel $BaWO_4$:Yb^{3+}/Ho^{3+}/Tm^{3+} nanophosphor by modulating sensitizer ion concentration. J. Mater. Sci.: Mater. Electron. **30**, 1068–1075 (2019)
8. C. Yang, X. Li, Q. Liu et al., Tunable white light emission of rare earth ions doped single matrix $SrAl_2Si_2O_8$ phosphors. J. Mater. Sci.: Mater. Electron. **31**, 1057–1064 (2020)
9. Y. Liu, G. Liu, J. Wang et al., Single-component and warm-white-emitting phosphor $NaGd(WO_4)_2$: Tm^{3+}, Dy^{3+}, Eu^{3+}: synthesis, luminescence, energy transfer, and tunable color. Inorg. Chem. **53**, 11457–11466 (2014)
10. N. Guo, Y. Huang, M. Yang et al., A tunable single-component warm white-light $Sr_3Y(PO_4)_3$: Eu^{2+}, Mn^{2+} phosphor for white-light emitting diodes. Phys. Chem. Chem. Phys. **13**, 15077–15082 (2011)
11. A. Santra, K. Panigrahi, S. Saha et al., Enhancement of radiative transitions in Sm^{3+} activated $CaTiO_3$ nanophosphor by modulating co-activator concentration. J Mater. Sci.: Mater. Electron. **30**, 6311–6321 (2019)
12. S. Mondal, J. Sarkar, S. Panja et al., Tuning visible emission from red to yellow of $PbWO_4$: Yb^{3+}/Ho^{3+} nanophosphor by modulating activator ion concentration. J. Phy. Chem. Sol. **129**, 442–447 (2019)
13. D. Geng, G. Li, M. Shang et al., Nanocrystalline $CaYAlO_4$:Tb^{3+}/Eu^{3+} as promising phosphors for full-color field emission displays. Dalton Trans. **41**, 3078–3086 (2012)
14. A.K. Dey, B. Samanta, P. Bhaumik et al., Low-temperature synthesis of thermally stable $BaWO_4$:Yb^{3+}:Ho^{3+} nanophosphors: tuning visible emission by controlling activator ion concentration. J. Lumin. **211**, 251–257 (2019)
15. B.K. Gupta, D. Haranath, S. Saini et al., Synthesis and characterization of ultra-fine Y_2O_3:Eu^{3+} nanophosphors for luminescent security ink applications. Nanotechnology **21**, 55607 (2010)

16. R. Yadav, A.F. Khan, A. Yadav et al., Intense red-emitting $Y_4Al_2O_9$:Eu^{3+}phosphor with short decay time and high color purity for advanced plasma display panel. Opt. Express **17**, 22023–22030 (2009)
17. M. Saraf, P. Kumar, G. Kedawat et al., Probing highly luminescent europium-doped lanthanum orthophosphate nanorods for strategic applications. Inorg. Chem. **54**, 2616–2625 (2015)
18. A. Kumar, G. Kedawat, P. Kumar et al., Sunlight-activated Eu^{2+}/Dy^{3+} doped $SrAl_2O_4$ water resistant phosphorescent layer for optical displays and defence applications. New J. Chem. **39**, 3380–3387 (2015)
19. B. Shao, Y. Feng, M. Jiao et al., Two-step synthetic route to GdOF:Ln^{3+} nanocrystals with multicolor luminescence properties. Dalton Trans. **45**, 2485–2491 (2016)
20. C. Li, P. Ma, P. Yang et al., Fine structural and morphological control of rare earth fluorides REF_3 (RE=La–Lu, Y) nano/microcrystals: microwave-assisted ionic liquid synthesis, magnetic and luminescent properties. CrystEngComm **13**, 1003–1013 (2011)
21. X.Y. Chen, C. Ma, X.X. Li et al., Novel necklace-like MAl_2O_4:Eu^{2+}, Dy^{3+} (M = Sr, Ba, Ca) phosphors via a CTAB-assisted solution-phase synthesis and postannealing approach. J. Phys. Chem. C **113**, 2685–2689 (2009)
22. R. Wiglusz, T. Grzyb, Sol−Gel synthesis of micro and nanocrystalline $BaAl_2O_4$:Eu^{3+} powders and their luminescence properties. Opt. Mater. **36**, 539–545 (2013)
23. B. Qu, B. Zhang, L. Wang et al., Mechanistic study of the persistent luminescence of $CaAl_2O_4$:Eu. Nd. Chem. Mater. **27**, 2195–2202 (2015)
24. K. Panigrahi, S. Saha, S. Sain et al., White light emitting $MgAl_2O_4$: Dy^{3+}, Eu^{3+} nanophosphor for multifunctional applications. Dalton Trans. **47**, 12228–12242 (2018)
25. T. Peng, L. Huajun, H. Yang et al., Synthesis of $SrAl_2O_4$:Eu, Dy phosphor nanometer powders by sol–gel processes and its optical properties. Mater. Chem. Phys. **85**, 68–72 (2004)
26. F. Clabau, X. Rocquefelte, S. Jobic et al., Mechanism of phosphorescence appropriate for the long-lasting phosphors Eu^{2+}-doped $SrAl_2O_4$ with codopants $Dy^{3+}$and B^{3+}. Chem. Mater. **17**, 3904–3912 (2005)
27. D.P. Bisen, R. Sharma, Mechanoluminescence properties of $SrAl_2O_4$:Eu^{2+} phosphor by combustion synthesis. Luminescence **31**, 394–400 (2016)
28. B.C. Jamalaiah, M. Jayasimhadri, Tunable luminescence properties of $SrAl_2O_4$: Eu^{3+} phosphors for LED applications. J. Mol. Struct. **1178**, 394–400 (2018)
29. M. Nazarov, M.G. Brik, D. Spassky et al., Crystal field splitting of 5d states and luminescence mechanism in $SrAl_2O_4$:Eu^{2+} phosphor. J. Lumin. **182**, 79–86 (2017)
30. J. Hölsä, T. Laamanen, M. Lastusaari et al., Electronic structure of the $SrAl_2O_4$:Eu^{2+} persistent luminescence material. J. Rare Earths **27**, 550–554 (2009)
31. V. Vitola, D. Millers, K. Smits et al., The search for defects in undoped $SrAl_2O_4$ material. Opt. Mater. **87**, 48–52 (2019)
32. H. Terraschke, M. Suta, M. Adlung et al., $SrAl_2O_4$:Eu^{2+}(-Dy^{3+}) nanosized particles: synthesis and interpretation of temperature-dependent optical properties. J. Spec. (2015). https://doi.org/10.1155/2015/541958
33. S. Saha, S. Das, U.K. Ghorai et al., Charge compensation assisted enhanced photoluminescence derived from Li-codoped $MgAl_2O_4$:Eu^{3+} nanophosphors for solid state lighting applications. Dalton Trans. **42**, 12965 (2013)
34. S. Saha, S. Das, U.K. Ghorai et al., Controlling nonradiative transition centers in Eu^{3+} activated $CaSnO_3$ nanophosphors through Na^+ co-doping: realization of ultrabright red emission along with higher thermal stability. J. Phys. Chem. C **119**, 16824–16835 (2015)
35. R. Chatterjee, S. Saha, D. Sen et al., Neutralizing the charge imbalance problem in Eu^{3+}-activated $BaAl_2O_4$ nanophosphors: theoretical insights and experimental validation considering K^+ codoping. ACS Omega **3**, 788–800 (2018)
36. S.K. Gupta, J.P. Zuniga, M. Abdou et al., Optical properties of undoped, Eu^{3+} doped and Li^+ co-doped $Y_2Hf_2O_7$ nanoparticles and polymer nanocomposite films. Inorg. Chem. Front. **7**, 505–518 (2020)
37. M. Yu, J. Lin, Z. Wang et al., Fabrication, patterning, and optical properties of nanocrystalline YVO_4: A (A = Eu^{3+}, Dy^{3+}, Sm^{3+}, Er^{3+}) phosphor films via sol-gel soft lithography. Chem. Mater. **14**, 2224–2231 (2002)